

Identification of Novel p38 α MAP Kinase Inhibitors Using Fragment-Based Lead Generation

Adrian L. Gill,^{†,*} Martyn Frederickson,[†] Anne Cleasby,[‡] Steven J. Woodhead,[†] Maria G. Carr,[†] Andrew J. Woodhead,[†] Margaret T. Walker,[†] Miles S. Congreve,[†] Lindsay A. Devine,[‡] Dominic Tisi,[‡] Marc O'Reilly,[‡] Lisa C. A. Seavers,^{||} Deborah J. Davis,^{||} Jayne Curry,^{||} Rachel Anthony,^{||} Alessandro Padova,^{§,⊗} Christopher W. Murray,[§] Robin A. E. Carr,[†] and Harren Jhoti[‡]

Astex Technology, 436 Cambridge Science Park, Milton Road, Cambridge, CB4 0QA, United Kingdom

Received June 3, 2004

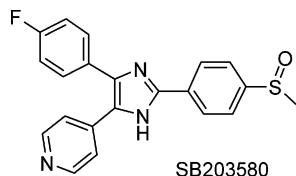
We describe the structure-guided optimization of the molecular fragments 2-amino-3-benzyl-oxypyridine **1** (IC₅₀ 1.3 mM) and 3-(2-(4-pyridyl)ethyl)indole **2** (IC₅₀ 35 μ M) identified using X-ray crystallographic screening of p38 α MAP kinase. Using two separate case studies, the article focuses on the key compounds synthesized, the structure–activity relationships and the binding mode observations made during this optimization process, resulting in two potent lead series that demonstrate significant increases in activity. We describe the process of compound elaboration either through the growing out from fragments into adjacent pockets or through the conjoining of overlapping fragments and demonstrate that we have exploited the mobile conserved activation loop, consisting in part of Asp168-Phe169-Gly170 (DFG), to generate significant improvements in potency and kinase selectivity.

Introduction

p38 α Mitogen-activated protein kinase (p38 α) is an intracellular serine/threonine (Ser/Thr) kinase that is activated by a range of environmental stimuli such as TNF- α , IL-1 β and stress.^{1,2} Activation of p38 α occurs through bis-phosphorylation on the Thr180-Gly181-Tyr182 motif located in the activation loop by dual-specificity Ser/Thr MAPK kinases, MKK3 and MKK6.^{2,3} In its activated state, p38 α phosphorylates a range of intracellular protein substrates which posttranscriptionally regulate the biosynthesis of TNF- α and IL-1 β . The pathophysiological consequences of excessive production of TNF- α and IL-1 β are understood to be significant mediators in the progression of many inflammatory diseases such as rheumatoid arthritis,⁴ Crohn's disease,⁵ inflammatory bowel disease⁶ and psoriasis.⁷

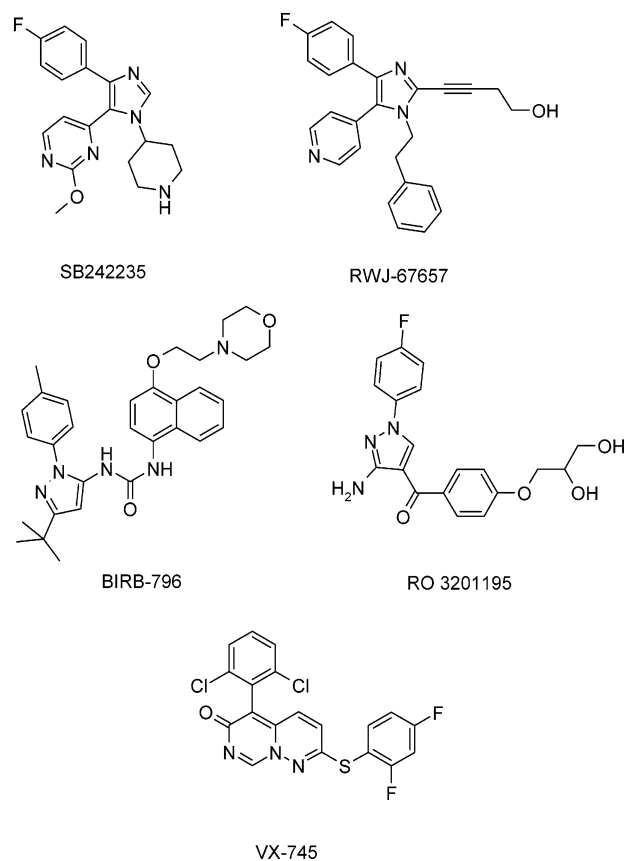
It has been demonstrated that inhibition of p38 α in mononuclear cells using SB203580 (Chart 1) signifi-

Chart 1. SB203580 p38 α MAP Kinase Inhibitor



cantly reduces TNF- α and IL-1 β production, providing strong evidence that it is a viable target for novel antiinflammatory therapy.^{8,9} To date, there are two marketed antiinflammatory agents that specifically

Chart 2. Structures of p38 α MAP Kinase Inhibitors That Have Advanced into Clinical Trials



inhibit TNF- α production, Enbrel (Etanercept), a soluble TNF- α receptor from Immunex^{10,11} and Remicade (Infliximab), a human TNF monoclonal antibody developed^{12,13} by Johnson & Johnson/Centocor, both of which are administered parenterally. The development of orally bioavailable small molecule inhibitors of p38 α would be greatly preferred in terms of ease of administration, patient compliance and expense. A number

* To whom correspondence should be addressed. Phone: +44 (0)-1223 226281; Fax +44 (0)1223 226201; E-mail: a.gill@astex-technology.com.

[†] Medicinal Chemistry group.

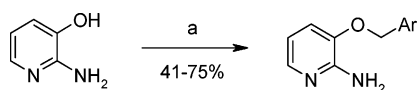
[‡] Protein Structure group.

[‡] Protein Technology group.

^{||} Biology group.

[§] Computational Chemistry and Informatics group.

[⊗] Current address: C4T, Colosseum Combinatorial Chemistry Centre for Technology, University of Rome 'Tor Vergata', Rome, Italy.

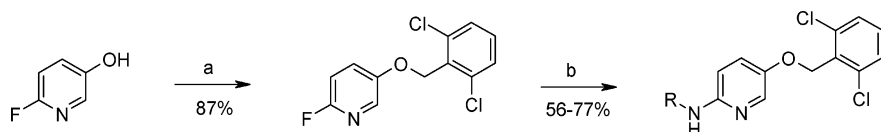
Scheme 1^a

^a Reagents: (a) Aryl halide, Adogen 464, aqueous 40% NaOH, CH₂Cl₂, 25 °C.

of promising orally bioavailable small molecule inhibitors have subsequently entered human clinical trials over recent years and have shown favorable pharmacokinetic and pharmacodynamic properties (Chart 2).^{14–17}

In the preceding paper¹⁸ we have described how high-throughput X-ray crystallographic screening can be used to identify low-affinity fragment hits for a range of targets. While these fragment hits have only low potency (μ M to mM), they are deemed to exhibit 'high efficiency' binding given their low molecular weights (100–250 Da) and limited levels of functionality. In this study we describe the structure-guided chemistry strategy that was employed to transform two such fragment hits into potent compounds having 'lead like' properties.¹⁹ Our strategy relies on obtaining many protein–ligand cocrystal structures to guide iterative cycles of hit optimization.^{20,21}

2-Amino-3-benzyloxy pyridine **1** (IC₅₀ 1.3 mM) and 3-(2-(4-pyridyl)ethyl)indole **2** (IC₅₀ 35 μ M) were identified from X-ray crystallographic screening of nonphosphorylated p38 α MAP kinase (Chart 3). Fragments **1** and **2** were chosen for optimization primarily due to their chemical tractability and novel binding modes. The structure-guided optimization of these two fragments is outlined in two separate case studies. In each case we describe the key compounds synthesized together with pertinent details concerning the observed crystallographic binding modes of more advanced compounds, culminating in two structurally distinct, novel and potent lead series.

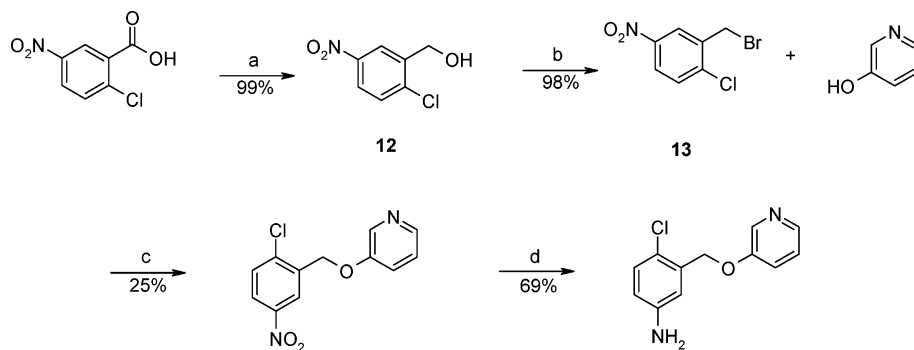
Scheme 2^a

11

6 R = NHCH₂CH₂OH

7 R = NH(CMe)₂CH₂OH

^a Reagents: (a) 2,6-Dichlorobenzyl chloride, NaH, DMF, ^tBu₄NCl, 25 °C. (b) 2-Aminopropan-1-ol, 130 °C or 2-amino-2-methylpropan-1-ol, 130 °C.

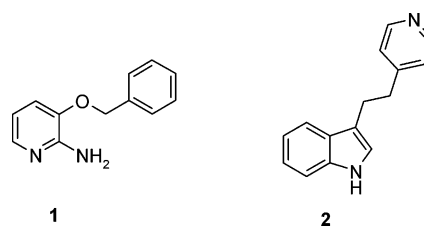
Scheme 3^a

14

15

^a Reagents: (a) BF₃·OEt₂, NaBH₄, THF, 0 °C. (b) PPh₃, CBr₄, 0 °C. (c) NaH, DMF, 0 °C. (d) Fe, FeSO₄·7H₂O, dioxane:water (5:1), reflux.

Chart 3



Case Study I. Fragment **1** binds to the previously described hinge region of the ATP binding site forming the well-documented hydrogen bond with the main chain amide nitrogen of Met109.²² As expected for such a low molecular weight compound, **1** demonstrated very low in vitro potency against p38 α (IC₅₀ 1.3 mM), however, the synthetic tractability and clearly defined binding mode of this molecule made it a valuable start point to initiate structure-guided fragment optimization.

Chemistry. Compound **3** (the des-amino derivative of **1**) is commercially available. Initial modifications to the phenyl ring of **1** led us to prepare compounds such as **4** and **5** (Table 3) which were readily synthesized by regioselective alkylation of 2-amino-3-hydroxypyridine upon treatment with the appropriate benzyl halides under phase-transfer conditions in the presence of catalytic amounts of Adogen 464 (Scheme 1).²³ Exploration of the lipophilic S1 subsite was achieved through compounds **6** and **7** which were synthesized from 2-amino-1-propanol or 2-amino-2-methyl-1-propanol using the known nucleophilic displacement chemistry of 2-fluoro-5-(2,6-dichlorobenzyl)pyridine **11** (Scheme 2).²⁴

Structural observations (discussed later) suggested accessing a range of target compounds with either amide or urea groups attached para to an aromatic ring halogen as exemplified by **8–10**. The necessary amine precursor **15** for these derivatives was accessed via the route outlined in Scheme 3. Boron trifluoride etherate-

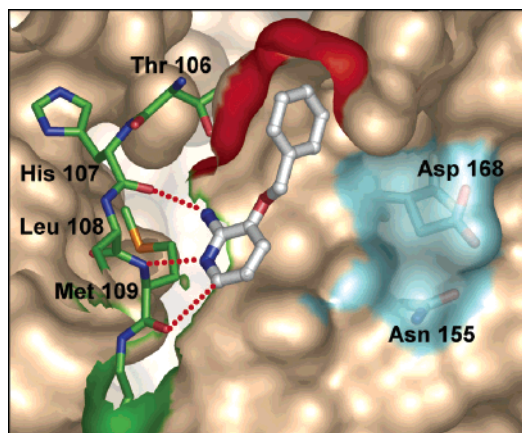


Figure 1. The p38 α MAP kinase ATP binding site. The hydrophobic region 1 (red), which is not occupied by ATP, is a known key specificity pocket.²⁶ Region 2 (green) is also hydrophobic and accommodates aliphatic moieties on inhibitors which contain terminal polar groups to modulate potency and physicochemical properties. The ribose binding region (blue) contains the amino acids that interact with the hydroxyl groups of the ribose of ATP. Fragment **1** is outlined in gray and shown making key hydrogen bond contacts (red dotted lines) to hinge residues.

mediated borohydride reduction of 2-chloro-5-nitrobenzoic acid gave alcohol **12**. Conversion to the bromomethyl derivative **13** was effected with $\text{CBr}_4/\text{PPh}_3$, and the crude product was treated with the alkoxy anion of 3-hydroxypyridine to furnish **14**. The nitro group of **14** was reduced to the corresponding aniline **15** using iron/iron sulfate in aqueous dioxane.

To evaluate the role of amide and urea linkages from the central aromatic ring, the synthesis of several analogues were undertaken. Amide bond formation was readily achieved using EDCI-mediated condensation of aniline **15** with the appropriate benzoic acids (Scheme 4); exposure of **15** to EDCI, HOAt and benzoic acid furnished amide **8**. Urea formation was accomplished upon treatment of the appropriate aminopyrazoles with triphosgene (Scheme 5). Thus treatment of **15** with triphosgene and 5-*tert*-butyl-2*H*-pyrazol-3-ylamine afforded urea **10**.

Results and Discussion

The architecture of the adenosine 5'-triphosphate (ATP) binding site of protein kinases is structurally well

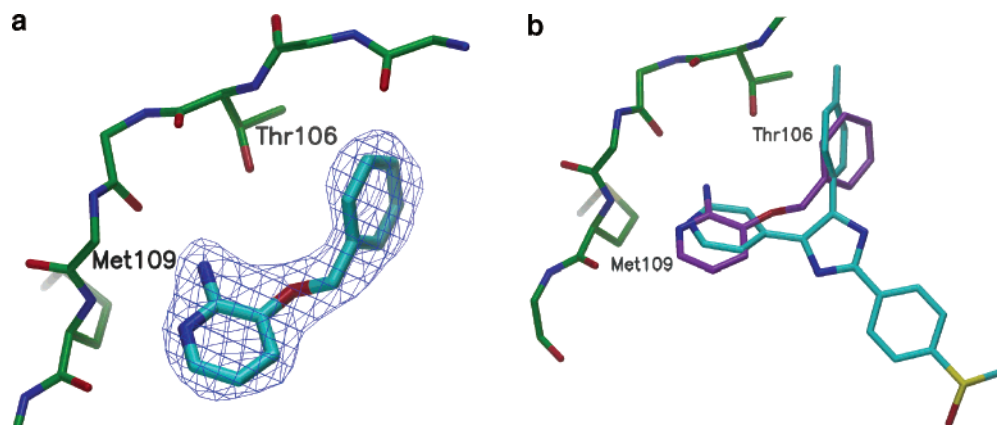
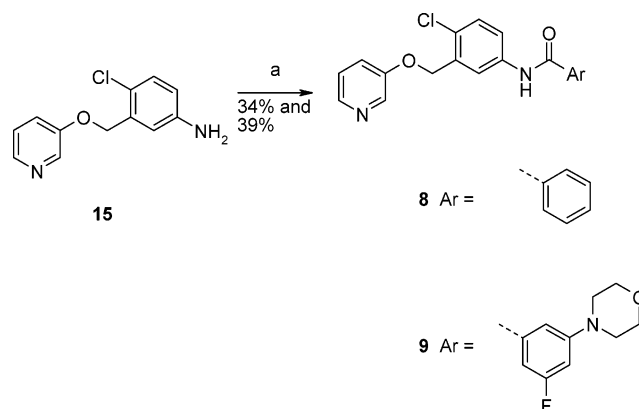


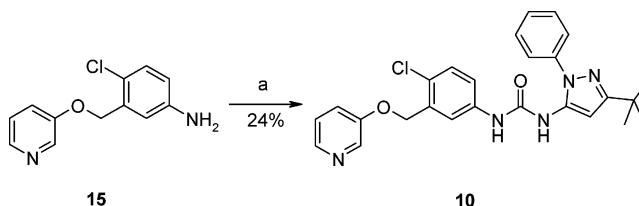
Figure 2. Ligand-bound crystal structure of p38 α MAP kinase. a. Omit map showing difference electron density (contoured at 3σ) for **1** bound to the hinge region of p38 α . b. Superposition (using C α coordinates of the respective proteins) of 4-[5-(4-fluorophenyl)-2-(4-methanesulfinylphenyl)-1*H*-imidazol-4-yl]pyridine (cyan) onto **1** (purple).

Scheme 4^a



^a Reagents: (a) EDCI, HOAt, CH_2Cl_2 , 25 °C, ArCO_2H .

Scheme 5^a



^a Reagents: (a) $\text{O}(\text{COCCl}_3)_2$, Et_2NiPr , CH_2Cl_2 , 0 °C, then 5-*tert*-butyl-2*H*-pyrazol-3-ylamine.

understood.²⁵ To facilitate our medicinal chemistry efforts, we analyzed the plethora of published structural data for p38 α alongside our own, to effectively navigate the ATP binding site and improve the affinity and selectivity of fragment **1** (Figure 1).

Pyridine **1** is a competitive inhibitor of p38 α MAP kinase with respect to ATP. The X-ray crystal structure of p38 α MAP kinase complexed with fragment hit **1** was solved to 2.2 Å resolution and demonstrates a clearly defined binding mode (Figure 2a) where **1** interacts with the hinge region located between the N- and C-terminal lobes of the kinase. The inhibitor makes hydrogen bond interactions through the pyridyl nitrogen to the NH of Met109 and the 2-amino moiety to the His107 backbone carbonyl. In addition, **1** forms a $\text{CH}\cdots\text{O}$ hydrogen bond through the pyridyl C6 hydrogen to the backbone carbonyl of Met109.²⁶ The benzyloxy group also makes a major interaction by filling the lipophilic specificity pocket (Figure 1).

Table 1. Data Collection Statistics for the Protein–Inhibitor Complexes Solved^a

compound	1	5	9	10	16	2	22	23	24
X-ray source	in-house	in-house	in-house	SRS 14.1	ESRF14.1	in-house	ESRF14.1	ESRF14.1	ESRF14.1
resolution (Å)	2.2	2.4	2.5	2.4	2.2	2.2	2.0	2.0	2.0
R_{merge}	0.063(0.131)	0.129(0.454)	0.15(0.43)	0.083(0.252)	0.088(0.266)	0.066(0.176)	0.045(0.145)	0.092(0.195)	0.107(0.347)
$I/\sigma(I)$	11.1(5.9)	6.2(2.2)	2.6(1.3)	6.7(2.3)	5.6(1.1)	12.5(7.5)	7.1(1.1)	4.8(2.6)	4.1(0.8)
completeness (%)	94.4(88.6)	78.7(58.8)	97.7(96.7)	96.2(93.2)	92.6(85.4)	93.9(91.4)	93.7(83.2)	90.8(84.8)	97.5(95.0)
a (Å)	45.77	45.3	45.68	46.14	45.68	45.64	45.5	45.77	45.35
b (Å)	87.10	85.91	86.10	86.00	85.37	86.60	86.86	85.3	85.46
c (Å)	126.34	125.71	126.07	125.73	126.00	124.92	125.20	126.64	125.60

^a $R_{\text{merge}} = \sum_{hkl} \sum_i |I_i(hkl) - I(hkl)| / \sum_{hkl} \sum_i I_i(hkl)$ where $I_i(hkl)$ is the intensity of an individual measurement, and $I(hkl)$ is the mean intensity of this reflection.

Table 2. Refinement Statistics^a

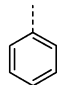
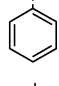
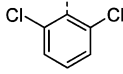
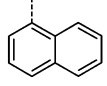
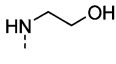
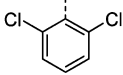
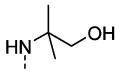
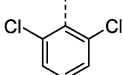
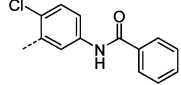
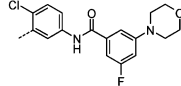
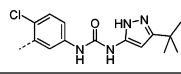
compound	1	2	5	9	10	16	22	23	24
resolution (Å)	19.7–2.2	19.6–2.2	29–2.4	19.9–2.5	43.3–2.4	50.7–2.2	43–2.05	38–1.97	42.7–2.0
R_{factor}	0.19	0.15	0.19	0.24	0.18	0.17	0.21	0.22	0.25
R_{free}	0.24	0.22	0.28	0.31	0.24	0.24	0.25	0.25	0.30
RMS bonds (Å)	0.005	0.013	0.005	0.006	0.005	0.004	0.007	0.008	0.008
RMS angles(deg)	0.86	1.27	0.85	0.96	0.85	0.79	1.3	1.27	1.3

^a $R_{\text{factor}} = \sum ||F_{\text{obs}}| - |F_{\text{calc}}|| / \sum |F_{\text{obs}}|$ where F_{obs} and F_{calc} are respectively the observed and calculated structure factors. R_{free} was calculated from 5% of the data excluded from refinement. Coordinates have been deposited with the PDB.³³

The binding mode of the p38 α inhibitor 4-[5-(4-fluorophenyl)-2-(4-methanesulfinylphenyl)-1*H*-imidazol-4-yl]pyridine was compared with that of **1** (Figure 2b). There is significant overlap of the two inhibitors with both making interactions through their pyridyl moieties via hydrogen bonds with the NH of Met109 and their respective aromatic groups occupying the lipophilic specificity pocket; however, despite some functional group similarities there is over 18500-fold difference in their p38 α MAP kinase activities. Analysis of the X-ray structure of **1** suggested that our initial efforts to increase potency of this low affinity fragment should focus on improving inhibitor interactions with the lipophilic specificity pocket. Appropriate space filling of this pocket has been shown to confer large increases in affinity and selectivity.^{15–17,27} Substitution of the phenyl ring of **1** with a 2,6-dichloro substitution pattern proved optimal (**4**, IC_{50} 109 μ M) affording an increase in potency of over 10-fold (Table 3). A further improvement in affinity for p38 α was gained through replacement of the benzyl group of **1** with a 1-naphthyl group (Figure 3). Addition of this moiety (**5**, IC_{50} 44 μ M) resulted in a 30-fold increase in potency over **1** by virtue of the increased number of hydrophobic contacts in the lipophilic specificity pocket. Despite the superior increase in activity conferred by the 1-naphthyl group, the 2,6-dichloro substitution was advanced instead since it offered the best balance of potency and physicochemical properties. Despite being involved through hydrogen bonding to the carbonyl of His107, the 2-amino substituent of **1** was found to be unnecessary for intrinsic p38 α activity as demonstrated by des-amino compounds, such as **3** (IC_{50} 1 mM), and was thus removed from subsequent analogues. The X-ray structure of **1** instead suggested that accessing the hydrophobic region 2 (Figure 1) with appropriate functionality might increase inhibitor activity. Indeed, substitution in the pyridine ring para to the 2,6-dichlorobenzoyloxy group was found to be tolerated, and the *gem*-dimethylethanolamine derivative **7** gave an increase in activity compared to **4**, albeit only 4-fold.

To explore alternative routes for optimization of fragment **1**, we synthesized and solved the protein–ligand complexes of a number of key compounds described in the prior art in order to understand more fully the interactions made by these potent inhibitors. Syn-

Table 3. Activities of **1** and **3–10** against p38 α MAP Kinase

Compound	R	R'	Ar	IC_{50} (μ M) ^a
SB203580				0.29
1	NH ₂	H		1300
3	H	H		1000
4	NH ₂	H		109
5	NH ₂	H		44
6	H			200
7	H			24
8	H	H		30
9	H	H		0.065
10	H	H		0.35

^a Average of two or more determinations.

thesis of the known urea **16** (Chart 4, IC_{50} 196 nM) and subsequent soaking into p38 α MAP kinase crystals revealed a unique binding mode for this compound (Figure 4a).²⁸ A significant conformational rearrange-

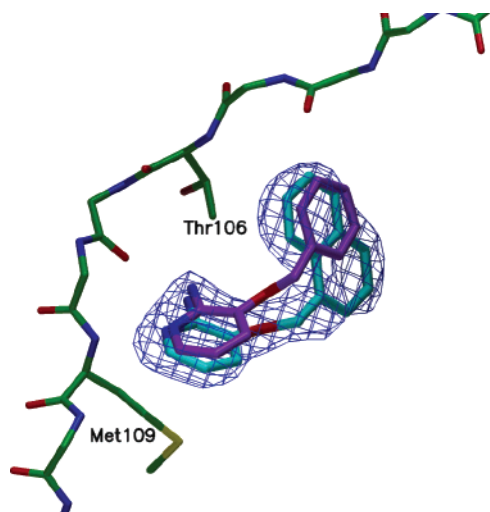
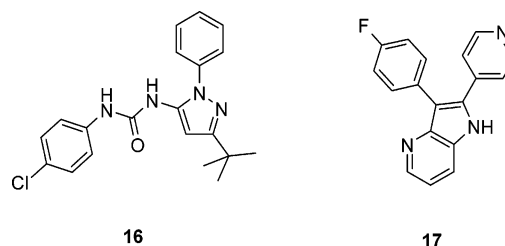


Figure 3. Omit map showing difference electron density (contoured at 3σ) for **5** bound to the hinge region of p38 α . Compound **1** (purple) is shown superposed onto **5** (cyan).

ment of the residues Asp168-Phe169-Gly170 (DFG motif) in the conserved activation loop of the kinase was induced, revealing a polar channel formed by Asp168 and Glu71 from the ATP binding site to a lipophilic pocket formed by the approximate 10 Å movement of Phe169. Overlaying X-ray crystal structures of **16** with our inhibitors suggested a number of functional group

Chart 4



substitution opportunities from the 2- and 5-positions of the phenyl ring of **1** to improve potency and selectivity (Figure 4b).

Synthesis of a range of amide and urea analogues, including **8**, **9** and **10** (Table 3) allowed us to exploit this activation loop movement. Benzamide **8** (IC_{50} 30 μ M) was tolerated, but a significant potency improvement was made with amide **9** (IC_{50} 65 nM). The *tert*-butyl-substituted pyrazole urea **10** (IC_{50} 350 nM) also served as a useful template for us to develop analogues with nanomolar potency against p38 α MAP kinase. A large conformational change for the conserved residues of the DFG motif is required for binding of these amide and urea derivatives (**9** and **10**, Figures 5a and 5b). The Phe169 side chain has again moved approximately 10 Å to a new “DFG out” conformation, whereby the Phe169 side chain now shields access to the ATP binding site.²⁹ The polar channel formed by Asp168 and

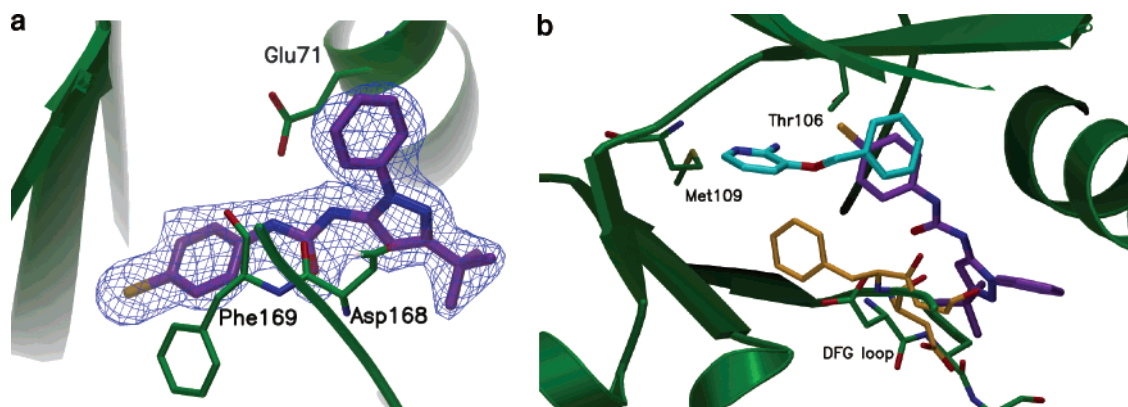


Figure 4. Ligand-bound crystal structure of p38 α MAP kinase. a. Omit map showing difference electron density (contoured at 3σ) for compound **16** bound to p38 α . b. Compound **1** (cyan) superposed on compound **16** (purple). The significant shift in the DFG loop (green for **1**, orange for **16**) is highlighted. Unlike **1**, **16** does not interact with the hinge region of the kinase.

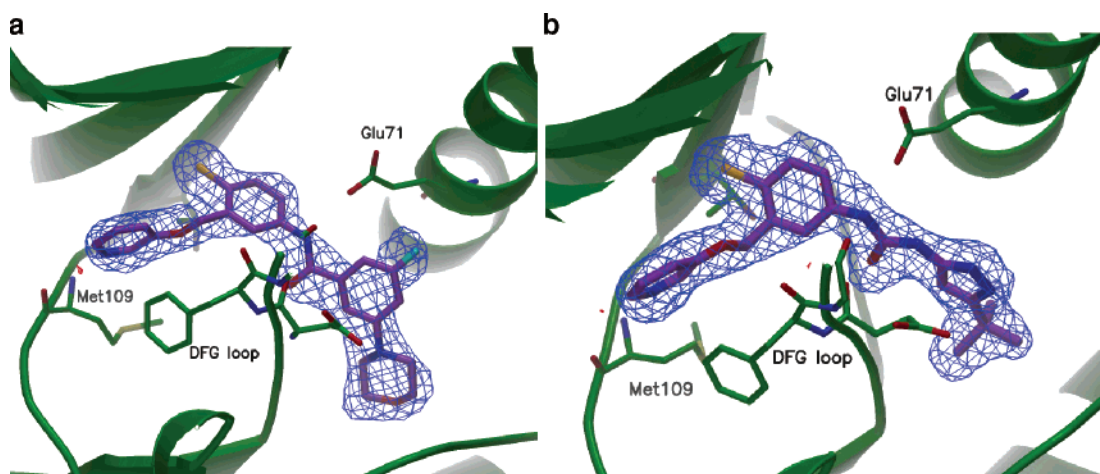
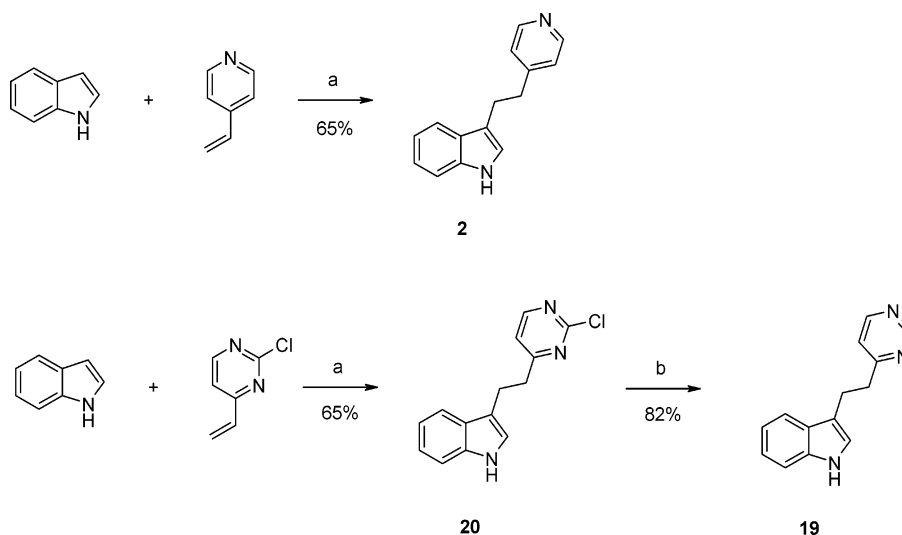


Figure 5. Ligand-bound crystal structure of p38 α MAP kinase. a. Omit map with difference electron density (contoured at 3σ) for **9** bound to p38 α . b. Omit map with difference electron density (contoured at 3σ) for **10** bound to p38 α .

Scheme 6^a

^a Reagents: (a) AcOH, 60–80 °C. (b) H₂, Pd/C, Et₃N, EtOH.

Table 4. Protein Kinase Selectivity Profile of **9**

kinase	kinase assay IC ₅₀ (μ M) ^a
p38 α	0.065
JNK-2 α 2	>10
ERK-1	>10
P56 ^{lck}	>10
CDK-2	>10
MAPKAP-2	>10

^a Average of two or more determinations

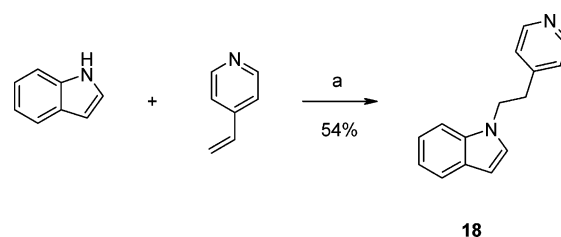
Table 5. Inhibition of TNF- α Release in THP-1 Cells by SB203580 and **9**

compound	THP-1 cell IC ₅₀ (μ M) ^a
SB203580	0.07
9	0.17

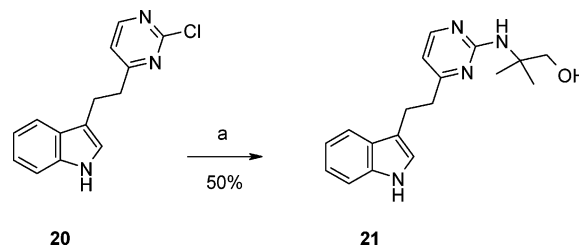
Glu71 from the ATP binding site to this allosteric pocket is involved in a hydrogen bond network to both the amide and urea functionalities. This movement of the Phe169 side chain exposes a largely lipophilic pocket into which the morpholine of amide **9** or the *tert*-butyl group of **10** may then insert. The morpholine and *tert*-butyl moieties respectively make substantial contacts with a number of neighboring hydrophobic residues; both **9** and **10** still maintain contacts to the hinge and lipophilic specificity pockets.

The selectivity profile of amide **9** against a panel of protein kinases was determined (Table 4). Overall, **9** appeared selective for p38 α MAP kinase, especially over the other stress-activated protein kinases JNK-2 and ERK-1. Examination of **9** for its effects on TNF- α secretion also proved promising; in an LPS-stimulated human fibroblast THP-1 cell assay **9** demonstrated good cellular potency (Table 5).

Case Study II. Fragment **2** also binds to the hinge region of the ATP binding site forming a hydrogen bond with the main chain amide nitrogen of Met109, with the 4-pyridyl and 3-indolyl moieties having a distinct gauche conformation about the central ethylene spacer.²⁹ Indole **2** demonstrated low in vitro inhibitory activity against p38 α (IC₅₀ 35 μ M) and is also a competitive inhibitor with respect to ATP. Once again, the synthetic tractability and well-defined binding mode of this frag-

Scheme 7^a

^a Reagents: (a) Na, CuSO₄, EtOH, 130 °C, sealed tube.

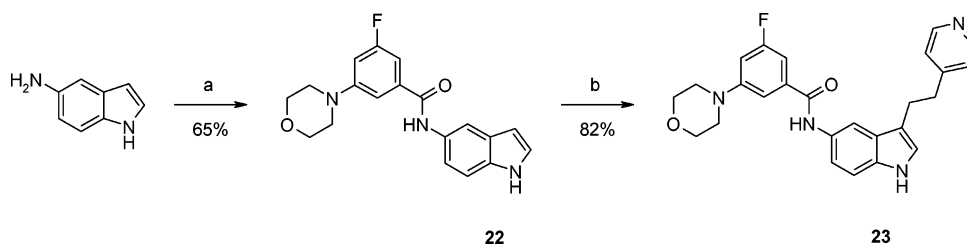
Scheme 8^a

^a Reagents: (a) 200 °C, 2-amino-2-methyl-1-propanol, microwave irradiation.

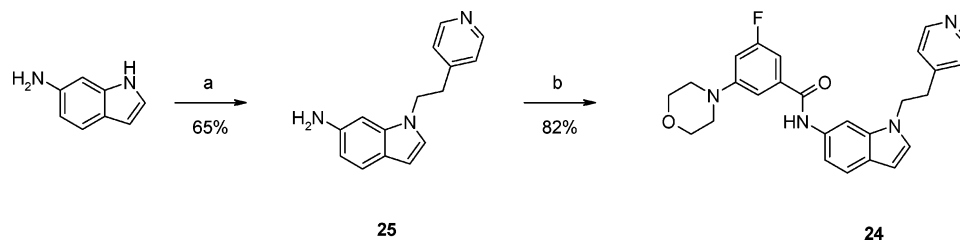
ment made it a suitable candidate to initiate structure-guided optimization chemistry.

Chemistry. Preparation of indole **2** was effected by reaction of indole with 4-vinylpyridine in refluxing acetic acid (Scheme 6).³⁰ To explore different hinge binding heterocycles, the pyrimidine variants **19** and **20** were prepared from 2-chloro-4-vinylpyrimidine in a manner analogous to that used for **2**. Catalytic hydrogenation of **20** under basic conditions furnished **19**. The isomeric indole derivative **18** was prepared by heating indole with 4-vinylpyridine in a sealed tube with metallic sodium and catalytic copper(II) sulfate (Scheme 7). Exploration of the lipophilic S1 subsite of p38 α was achieved with compounds such as **21** which was prepared from **20** and 2-amino-2-methyl-1-propanol using microwave irradiation-induced nucleophilic displacement conditions (Scheme 8).²⁴

Structural observations from optimization of fragment **1** (discussed above) suggested the preparation of amides **23** and **24** from the indole ring to exploit the mobile DFG

Scheme 9^a

^a Reagents: (a) EDCI, HOBt, DMF, 3-fluoro-5-morpholin-4-ylbenzoic acid, 25 °C. (b) 4-vinylpyridine, AcOH, reflux.

Scheme 10^a

^a Reagents: (a) Na, CuSO₄, EtOH, 130 °C, 4-vinylpyridine, sealed tube. (b) EDCI, HOBt, DMF, 25 °C, 3-fluoro-5-morpholin-4-ylbenzoic acid.

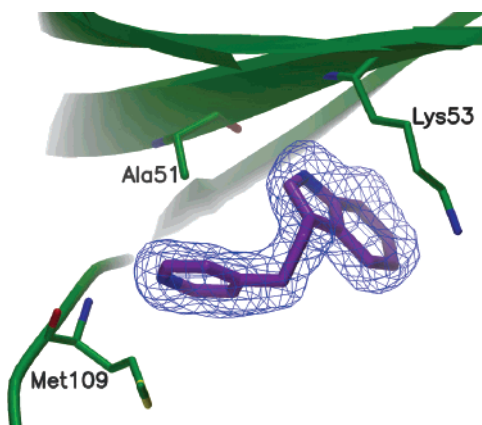


Figure 6. Omit map with difference electron density (contoured at 3σ) for **2** bound to p38 α . Key residues implicated in the binding of **2** are highlighted.

region of the kinase activation loop. Amide bond formation was readily achieved by EDCI-mediated condensation of 5-aminoindole or 6-amino-1-[2-(4-pyridyl)ethyl]-indole **25** with the appropriate benzoic acids (Schemes 9 and 10). Thus exposure of **25** to EDCI, HOBt and 3-fluoro-5-(4-morpholino)benzoic acid furnished amide **24**.

Results and Discussion

Indole **2** has a very clearly defined (2.3 Å resolution) crystallographic binding mode (Figure 6) with the 4-pyridyl moiety binding to the hinge region located between the N- and C-terminal lobes of the kinase. A novel binding feature of **2** is the interaction involving the 3-indolyl group in the specificity pocket of p38 α . The indole moiety is buried deep within this hydrophobic cleft, with both rings making substantial contacts with a number of neighboring residues, including the side chain methylenes of Lys53. In addition the indolyl NH acts as a hydrogen bond donor to the backbone carbonyl of Ala51 (~3.0 Å). Indoles (and related compounds) have been exemplified previously as inhibitors of p38 α MAP kinase; however, X-ray crystallographic studies suggest

them to have distinctly different binding modes to **2**.³¹ For example, the azaindole ring of **17** (Chart 4) does not bind in the kinase specificity pocket of p38 α ; instead the 4-fluorophenyl moiety occupies this key hydrophobic region.

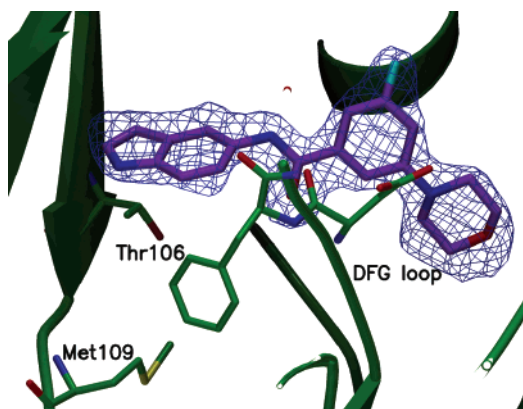
Numerous examples of p38 α inhibitors exist which contain a substituted monocyclic ring bound within the kinase specificity pocket. Despite p38 α being one of the most heavily investigated of kinases, indole **2** is, to the best of our knowledge, the first example of a bicyclic heterocycle that binds to the kinase with both rings buried deep within the hydrophobic specificity pocket. As such, we believe that **2** (and closely related analogues described herein) constitutes a novel and distinct class of inhibitors that have implications both for the design of inhibitors of p38 α and for kinases in general.

To optimize **2** we prepared a number of similar analogues including the isomeric N-substituted derivative **18** which was around 5-fold less active than **2** and had an essentially identical binding mode (not shown). The less basic pyrimidine **19** demonstrated a significant loss in potency compared to **2**. Previous studies have shown that the potency of hinge binding p38 α inhibitors can be enhanced by substitution at the 2-position of the key Met109 binding heteroaryl residue.³² Substituted pyrimidines **20** and **21** resulted in the desired increase in activity, with **21** demonstrating almost a 500-fold increase in potency compared to **19** (Table 6).

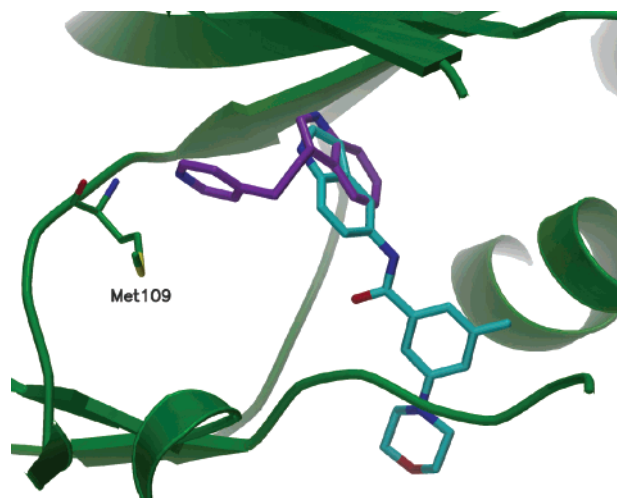
A novel binding mode coupled with a promising level of potency despite the low molecular weight of **2** led us to design a series of indole derived fragments based on the SAR and structural knowledge we had gained from optimizing fragment **1**. We envisaged that this would allow us to rationally elaborate **2**, thereby delivering large and rapid increases in potency. Indeed, targeting the DFG activation loop segment of the kinase with an aromatic amide-indole hybrid **22** (IC₅₀ 162 μ M) revealed the indole moiety to be again bound in the hydrophobic specificity pocket in the liganded crystal structure (Figure 7, 2.1 Å resolution data). Unlike **2**, **22** makes no contact with Met109 and instead forms two hydrogen

Table 6. Activities of **2** and **19–23** against p38 α MAP Kinase

Compound	R	R'	IC ₅₀ (μ M) ^a
SB203580			0.29
2	H		35
19	H		720
20	H		120
21	NH ₂		1.5
22		H	162
23			0.63

^a Average of two or more determinations.**Figure 7.** Omit map with difference electron density (contoured at 3σ) for **22** bound to p38 α .

bonds from the amide carbonyl and NH to the NH of Asp168 and a side chain oxygen of a salt bridging

**Figure 8.** Overlay of the X-ray crystal structures of **2** (purple) and **22** (cyan) highlighting both the overlap of the two indolyl moieties (located within the hydrophobic specificity pocket) and their position relative to Met109 at the hinge of p38 α .

Glu171 respectively (both ~ 3.0 Å). Significant conformational rearrangement (up to 11.6 Å) of the residues Asp168-Phe169-Gly170 in the kinase was again induced, with the aromatic side chain of Phe169 shielding the hydrophobic regions of **22** (H-6 and H-7 of the indole) from solvent. The morpholine group of **22** that is located within the pocket vacated by Phe169, again makes substantial contacts with a number of neighboring hydrophobic residues.

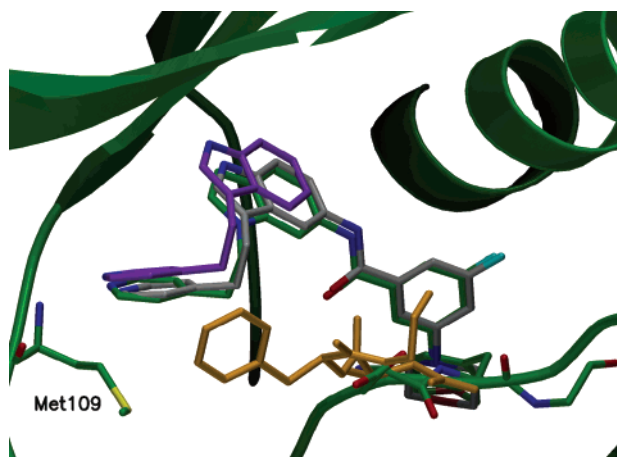
Amide **22** is unusual in that despite being only relatively small in size and possessing only moderate potency (IC₅₀ 162 μ M) it is still able to induce this conformational change. Urea **16** (IC₅₀ 196 nM) is also able to effect this conserved activation loop movement, but is somewhat larger and more lipophilic than **22**, accounting for its increased inhibitory activity. Comparison of the crystal structures of **2** and **22** (Figure 8) showed that the indole moieties were essentially overlapping and that, somewhat unexpectedly, the indolyl NH of **22** was not buried in the specificity pocket but was instead accessible to solvent and appeared to be useful as a vector with which to reach Met109. Given that the observed binding modes of **2** and **18** were essentially identical and that **18** contained an indole aligned similarly to that in **22**, we attempted to improve potency within the series by preparing derivatives arising from the conjoining of **2** or **18** with the overlapping fragment **22**.

The higher affinity for a lower molecular weight of **2** and **18** compared to **22** meant that we chose to retain the binding modes of **2** and **18** and to append added functionality present in **22**. X-ray crystallographic overlays suggested that 3,5- and 1,6-disubstituted indoles were likely to be effective; we therefore prepared amides **23** (IC₅₀ 630 nM) and **24** (IC₅₀ 340 nM). Both derivatives gave good increases in potency arising from maintaining the more efficient binding modes of **2** and **18** with the introduction of specific functionality from **22** to effect movement of the conserved DFG loop (Table 7).

X-ray crystallographic analysis of co-complexes of p38 α with **23** and **24** (both 2.0 Å resolution) showed them to have very similar binding modes (Figure 9; **23** shown in gray, **24** in green) as might be expected for

Table 7. Activities of **18** and **24** against p38 α MAP Kinase

Compound	R	IC ₅₀ (μ M) ^a
SB203580		0.29
18	H	185
24		0.34

^a Average of two or more determinations.**Figure 9.** Overlay of the X-ray crystal structures of **2** (purple), **23** (grey) and **24** (green). The mobile DFG loop is highlighted in green (for **2**) and yellow (for **23** and **24**).

regioisomers with essentially identical molecular geometries. The observed binding modes for both **23** and **24** are essentially a weighted average of **2** and **22**, with the indolyl moiety of each binding in the hydrophobic specificity pocket of p38 α . As expected, both compounds effect movement of the DFG loop to accommodate the morpholine functionality in a manner analogous to **22**.

Conclusions

The case studies outlined exemplify the potential of X-ray crystallographic screening and structure-guided fragment optimization to generate useful lead compounds. In case study I, we identified a potent and selective series of p38 α MAP kinase inhibitors starting from a millimolar affinity fragment **1** by employing structure-guided chemistry. The synthesis of analogues of **1** is brief and amenable to large scale, allowing for the rapid production of a wide range of derivatives. Initial attempts to improve potency were centered on the hydrophobic regions 1 and 2 (Figure 1), gaining over a 50-fold improvement in kinase activity for **7** over **1**.

Attempts to improve the potency of the series into the nanomolar range successfully exploited a binding pocket revealed by the large conformational movement of the conserved DFG binding loop. Compound **9** has druglike physicochemical properties, demonstrates over 100 fold selectivity over a panel of kinases and was able to potently inhibit the production of TNF- α from LPS-stimulated THP-1 cells. The encouraging early in vitro data generated from this series warrants further investigation in a range of animal models of inflammatory disease.

In case study II, we have described the discovery of a novel indole-derived series of inhibitors of p38 α MAP kinase that bind in a hitherto unprecedented mode with both rings of the indolyl moiety located within the hydrophobic specificity pocket. We have demonstrated that significant increases in potency (> 100 fold) can be realized extremely rapidly by conjuring a pair of overlapping fragment hits from X-ray crystallographic experiments and exploiting two key binding modes within the ATP binding site.

Upon the basis of these results, fragment based X-ray crystallographic screening shows particular promise as a new approach for the discovery and optimization of novel protein kinase inhibitors.

Experimental Section

Protein X-ray Crystallography. p38 α Protein (1 μ L) at a concentration of 8–14 mg/mL in 25mM HEPES, pH 7.5, 200 mM NaCl and 1mM DTT was mixed with 1 μ L of well solution containing 100 mM HEPES, pH 7.0, 200 mM (NH₄)₂SO₄ and 17% w/v PEGMME5000. Crystals were grown in hanging drops, using microseeding methods. Crystals of p38 α routinely grew in space group *P*2₁2₁2₁ (*a* = 45.01 Å, *b* = 84.82 Å, *c* = 125.42 Å) as previously described.³⁴

Compound **1** was discovered from a crystallographic screen of a fragment set as described earlier.¹⁸ The individual compound was then soaked into a p38 α and the crystal exposed to the compound at a concentration of 50mM in 10% DMSO mixed with a harvesting solution for 3 h. The crystal was then transferred to a cryoprotectant solution for 5–10 s and subsequently frozen in liquid nitrogen. Compounds **2**, **5**, **10**, **16**, **22**, **23** and **24** were treated in a similar way, and compound **9** was soaked at 1 mM in 5% DMSO/harvesting solution, prior to transfer to cryoprotectant and freezing.

Data were collected for these crystals, both in house, using a Jupiter CCD or an RAXISIV image plate detector mounted on a Rigaku rotating anode generator, or using synchrotron radiation sources (Table 1), and processed using D³trek³⁵ or MOSFLM.³⁶ Solution and refinement of complex structures was done using a semiautomated procedure which used an in-house apo structure as a starting model for molecular replacement, and subsequently consecutive rounds of refinement and water placement were done until convergence was reached. The refinement programs used were CNX³⁷ or REFMAC.³⁸ The ligands were placed in the difference density using Autosolve and further refinement was carried out.³⁹ Some rebuilding of parts of the molecule was necessary, and this was done using QUANTA(QUANTA96).⁴⁰ The refinement statistics are outlined in Table 2. The coordinates have been deposited in the Protein Structure Bank.³³

Synthetic Materials and Methods. Reagents and solvents were obtained from commercial suppliers and used without further purification. Thin-layer chromatography (TLC) analytical separations were conducted with E. Merck silica gel F-254 plates of 0.25 mm thickness and were visualized with UV light (254 nm) or I₂. Flash chromatography was performed according to the procedure of Still et al. (E. Merck silica gel, mesh). ¹H nuclear magnetic resonance (NMR) spectra were recorded in the deuterated solvents specified on a Bruker

Avance 400 spectrometer operating at 400 MHz. Chemical shifts are reported in parts per million (δ) from the tetramethylsilane resonance in the indicated solvent (TMS: 0.0 ppm). Data are reported as follows: chemical shift, multiplicity (br = broad, s = singlet, d = doublet, t = triplet, m = multiplet), coupling constants (Hz), integration. Compound purity and Mass spectra were determined by a Waters Fractionlynx/Micromass ZQ LC/MS platform using the positive electrospray ionization technique (+ES) using a mobile phase of acetonitrile/water with 0.1% formic acid.

2-Amino-3-(2,6-dichlorobenzoyloxy)pyridine (4). A mixture of 2-amino-3-hydroxypyridine (0.22 g, 2.00 mmol), 2,6-dichlorobenzoyl chloride (0.49 g, 2.14 mmol) and Adogen 464 (1 drop) in aqueous 40% NaOH solution (2 mL) and dichloromethane (2 mL) was stirred at room temperature for 24 h. The dichloromethane was separated and the aqueous layer diluted with water (10 mL) and then extracted with dichloromethane (3 \times 25 mL). The organic extracts were combined, dried (MgSO₄), filtered and concentrated. Recrystallization from hexane/dichloromethane gave 0.39 g of **4** as an off-white solid (69%). ¹H NMR (400 MHz, MeOD): δ 7.56 (d, J = 2 Hz, 1H), 7.49 (d, J = 8 Hz, 2H), 7.38 (dd, J = 8.1, 3.2 Hz, 1H), 7.29 (d, J = 7.9 Hz, 1H), 6.67 (m, 1H), 5.36 (s, 2H). MS (+ES): *m/e* 270 (MH⁺).

2-Amino-3-(1-naphthylmethoxy)pyridine (5). A mixture of 2-amino-3-hydroxypyridine (0.22 g, 2.00 mmol), 1-naphthylmethyl chloride (0.38 g, 2.20 mmol) and Adogen 464 (1 drop) in aqueous 40% NaOH solution (2 mL) and dichloromethane (2 mL) was stirred at room temperature for 19 h. The dichloromethane was separated and the aqueous layer diluted with water (10 mL) and then extracted with dichloromethane (3 \times 25 mL). The organic extracts are combined, dried (MgSO₄), filtered and concentrated. Purification by column chromatography, eluting with 5% ethyl acetate/petroleum ether, afforded 0.38 g of **5** as a cream solid (75%). ¹H NMR (400 MHz, CDCl₃): δ 4.63 (br s, 2H), 5.49 (s, 2H), 6.64 (dd, J = 8, 5 Hz, 1H), 7.12 (dd, J = 8, 1.5 Hz, 1H), 7.48 (dd, J = 8, 7 Hz, 2H), 7.55 (m, 2H), 7.71 (dd, J = 5, 1.5 Hz, 1H), 7.90 (m, 2H), 8.03 (m, 1H). MS (+ES): *m/e* 251 (MH⁺).

5-(2,6-Dichlorobenzoyloxy)-2-fluoropyridine (11). Sodium hydride (60% dispersion in oil, 0.265 g, 6.63 mmol) was added portionwise to a solution of 2-fluoro-5-hydroxypyridine (0.3 g, 2.65 mmol) in DMF (6 mL) at room temperature, under an atmosphere of nitrogen. After stirring for 45 min, 2,6-dichlorobenzoyl chloride (1.55 g, 7.96 mmol) and ⁿBu₄N⁺I⁻ (0.01 g, 0.26 mmol) were added, and the reaction mixture was stirred for a further 6 h. Water (5 mL) was added dropwise, and the reaction mixture was partitioned between ethyl acetate (50 mL) and brine (10 mL). The organic layer was separated, and the aqueous layer was extracted with ethyl acetate (2 \times 30 mL). The combined organic extracts were dried (MgSO₄), filtered and concentrated, and the residue was then purified by column chromatography, eluting with 5% ethyl acetate/petroleum ether, to yield 0.71 g of **11** as an off-white solid (99%). ¹H NMR (400 MHz, CDCl₃): δ 5.31 (s, 2H), 6.89 (dd, J = 8.8, 3.5 Hz, 1H), 7.27–7.31 (m, 1H), 7.39 (d, J = 8.3 Hz, 2H), 7.42–7.48 (m, 1H), 7.96 (d, J = 1.7 Hz, 1H). MS (+ES): *m/e* 273 (MH⁺).

2-[5-(2,6-Dichlorobenzoyloxy)-2-pyridinylamino]ethanol (6). A solution of **11** (0.132 g, 0.49 mmol) in ethanolamine (2.5 mL) was heated to 130 °C for 22 h. Upon cooling, the mixture was stirred with ethyl acetate (3 \times 25 mL) and the ethyl acetate layer was decanted. The combined organic extracts were dried (MgSO₄), filtered and concentrated. Purification by column chromatography, eluting with 50% ethyl acetate/petroleum ether, afforded 0.085 g of **6** as a pale yellow oil (56%). ¹H NMR (400 MHz, MeOD): δ 3.41 (t, J = 5.6 Hz, 2H), 3.73 (t, J = 5.6 Hz, 2H), 5.27 (s, 2H), 6.59 (dd, J = 9.1, 0.8 Hz, 1H), 7.31 (dd, J = 9.1, 2.9 Hz, 1H), 7.38 (dd, J = 8.8 and 7.1, 1H), 7.46 (s, 1H), 7.48 (d, J = 1.3 Hz, 1H), 7.76 (dd, J = 3.0, 0.8 Hz, 1H). MS (+ES): *m/e* 314 (MH⁺).

2-[5-(2,6-Dichlorobenzoyloxy)-2-pyridinylamino]-2-methyl-1-propanol (7). A solution of **11** (0.054 g, 0.198 mmol) in 1,1-dimethylethanolamine (1.5 mL) was heated to 130 °C for

72 h. Upon cooling, the mixture was partitioned with ethyl acetate (80 mL) and water (25 mL). The organic layer was dried (MgSO₄), filtered and evaporated to dryness. The residue was purified by column chromatography, eluting with 50% ethyl acetate/petroleum ether, to give 0.01 g of **7** as a yellow oil (15%). ¹H NMR (400 MHz, MeOD): δ 1.33 (s, 6H), 3.59 (s, 2H), 5.27 (s, 2H), 6.63 (dd, J = 9.1, 0.8 Hz, 1H), 7.27 (dd, J = 8.8, 2.8 Hz, 1H), 7.38 (dd, J = 8.8, 7.1 Hz, 1H), 7.46 (s, 1H), 7.48 (d, J = 1.3 Hz, 1H), 7.77 (d, J = 2.8 Hz, 1H), 8.58 (br s, 1H). MS (+ES): *m/e* 342 (MH⁺).

(2-Chloro-5-nitrophenyl)methanol (12). To a stirred suspension of sodium borohydride (0.375 g, 9.9 mmol) in dry THF (20 mL) at 0 °C was added 2-chloro-5-nitrobenzoic acid (0.999 g, 4.96 mmol) dissolved in dry THF (5 mL). Boron trifluoride etherate (1.69 mL, 13.3 mmol) was added dropwise and the reaction mixture allowed to warm to room temperature over 1 h. The reaction mixture was quenched with 1 N HCl and then partitioned between DCM and water. The organic layer was separated, washed with brine solution, dried (MgSO₄), filtered, and evaporated and the residue purified by column chromatography on silica. Elution with mixtures of petroleum ether and ethyl acetate afforded 0.92 g of **12** as an off-white solid (99%). ¹H NMR (400 MHz, CDCl₃): δ 8.5 (br s, 1H), 8.13 (br dd, 1H), 7.54 (d, J = 8 Hz, 1H), 4.89 (s, 2H). MS (+ES): *m/e* 189 (MH⁺).

2-Bromomethyl-1-chloro-4-nitrobenzene (13). A solution of **12** (0.916 g, 4.9 mmol) in DCM (30 mL) was cooled to 0 °C and triphenylphosphine (1.31 g, 5 mmol) was added followed by carbon tetrabromide (1.63 g, 4.9 mmol). The reaction mixture was stirred at room temperature for 24 h and then diluted with DCM and washed with water followed by brine solution. The organic layer was separated, dried (MgSO₄), filtered and evaporated to yield 1.21 g of pure **13** as a pale yellow oil (98%). ¹H NMR (400 MHz, CDCl₃): δ 8.37 (br s, 1H), 8.15 (dd, J = 8, 1 Hz, 1H), 7.61 (d, J = 8 Hz, 1H), 4.63 (s, 2H). MS (+ES): *m/e* 252 (MH⁺).

3-(2-Chloro-5-nitrobenzoyloxy)pyridine (14). 3-Hydroxypyridine (0.5 g, 5.3 mmol) was dissolved in dry DMF (6 mL), cooled to 0 °C and then treated with sodium hydride (60%, 5.5 mmol). After 0.2 h, **13** (1.22 g, 4.9 mmol) was added in dry DMF (6 mL) and the reaction mixture stirred at 0 °C for 1 h. The reaction mixture was quenched with water and then partitioned between ethyl acetate and water. The organic layer was separated, washed with brine solution, dried (MgSO₄), filtered, and evaporated and the residue purified by column chromatography on silica. Elution with mixtures of petroleum ether and ethyl acetate afforded 0.32 g of **14** as a cream solid (25%). ¹H NMR (400 MHz, CDCl₃): δ 8.47 (dd, J = 12.9, 1.8 Hz, 2H), 8.33 (d, J = 4.5 Hz, 1H), 8.17 (dd, J = 9.3, 2.3 Hz, 1H), 7.61 (d, J = 8.8 Hz, 1H), 7.38 (m, 2H), 5.26 (s, 2H). MS (+ES): *m/e* 266 (MH⁺).

3-(5-Amino-2-chlorobenzoyloxy)pyridine (15). A solution of **14** (0.317 g, 1.2 mmol) in dioxane:water (5:1, 6 mL) was treated with iron powder (0.609 g, 10.9 mmol) and iron sulfate heptahydrate (0.74 g, 2.66 mmol). The reaction mixture was refluxed for 6 h, cooled to room temperature and filtered. The filtrate was diluted with ethyl acetate and washed with saturated sodium bicarbonate and then brine solution. The organic layer was separated, dried (MgSO₄), filtered and evaporated to give 0.195 g of **15** as a dark brown oil (69%) and used in subsequent reactions without further purification. ¹H NMR (400 MHz, CDCl₃): δ 8.71 (d, J = 3 Hz, 1H), 8.48 (d, J = 5.3 Hz, 1H), 8.07 (br d, 1H), 7.85 (dd, J = 8.8 Hz, 1H), 7.41 (d, J = 8.3 Hz, 1H), 7.23 (s, 1H), 7.06 (d, J = 8.1 Hz, 1H), 5.37 (s, 2H). MS (+ES): *m/e* 236 (MH⁺).

N-[4-Chloro-3-(3-pyridinylloxymethyl)phenyl]benzamide (8). A stirred solution of **15** (0.033 g, 0.14 mmol) in dry DCM (5 mL) was treated with 1-(3-dimethylaminopropyl)-3-ethylcarbodiimide hydrochloride (0.322 g, 1.68 mmol) and 1-hydroxy-7-azabenzotriazole (0.229 g, 1.68 mmol). Benzoic acid (0.017 g, 0.14 mmol) was added and the reaction mixture stirred at room temperature overnight. The reaction mixture was then diluted with DCM and washed with 5% aqueous citric acid, saturated sodium bicarbonate solution and finally

brine solution. The organic layer was separated, dried (MgSO₄), filtered, and evaporated and the residue purified by column chromatography on silica. Elution with mixtures of petroleum ether and ethyl acetate afforded 0.021 g of **8** as an off-white solid (34%). ¹H NMR (400 MHz, CDCl₃): δ 8.47 (br s, 1H), 8.29 (br s, 1H), 8.2 (br s, 1H), 7.9 (br m, 3H), (7.74 (br m, 2H), 7.63 (br m, 1H), 7.52 (br m, 3H), 7.43 (d, *J* = 8.8 Hz, 1H), 5.31 (s, 2H). MS (+ES): *m/e* 340 (MH⁺).

N-[4-Chloro-3-(3-pyridinyloxymethyl)phenyl]-3-fluoro-5-(4-morpholino)-benzamide (9). A stirred solution of **15** (0.047 g, 0.2 mmol) in dry DCM (5 mL) was treated with 1-(3-dimethylaminopropyl)-3-ethylcarbodiimide hydrochloride (0.383 g, 2 mmol) and 1-hydroxy-7-azabenzotriazole (0.272 g, 2 mmol). 3-Fluoro-5-(4-morpholino)benzoic acid (0.045 g, 0.2 mmol) was added and the reaction mixture stirred at room-temperature overnight. The reaction mixture was diluted with DCM and washed with 5% aqueous citric acid, saturated sodium bicarbonate solution and then brine solution. The organic layer was separated, dried (MgSO₄), filtered, and evaporated and the residue purified by column chromatography on silica. Elution with mixtures of petroleum ether and ethyl acetate afforded 0.035 g of **9** as a pale yellow solid (39%). ¹H NMR (400 MHz, CDCl₃): δ 8.42 (br s, 1H), 8.23 (d, *J* = 4.8 Hz, 1H), 8.12 (s, 1H), 7.76 (m, 2H), 7.35 (m, 3H), 7.20 (s, 1H), 6.95 (d, *J* = 8.3 Hz, 1H), 6.71 (m, 1H), 5.22 (s, 2H), 3.84 (t, *J* = 9.9, 4.8 Hz, 4H), 3.21 (t, *J* = 9.9, 4.8 Hz, 4H). MS (+ES): *m/e* 443 (MH⁺).

1-(5-tert-Butyl-2H-pyrazol-3-yl)-3-[4-chloro-3-(pyridin-3-ylloxymethyl)-phenyl]urea (10). A stirred solution of **15** (0.049 g, 0.21 mmol) in dry DCM (5 mL) at 0 °C was treated with *N,N*-diisopropylethylamine (0.37 mL, 2.13 mmol), followed by triphosgene (0.077 g, 0.25 mmol). The mixture was stirred at 0 °C for 3 h and then treated with 3-amino-5-*tert*-butyl pyrazole (0.058 g, 0.42 mmol). The reaction mixture was allowed to warm to room-temperature overnight, the solvent was removed under reduced pressure and the residue partitioned between ethyl acetate and saturated sodium bicarbonate solution. The organic layer was separated, dried (MgSO₄), filtered, and evaporated and the residue purified by column chromatography on silica. Elution with mixtures of petroleum ether and ethyl acetate afforded 0.02 g of **10** as a pale yellow solid (24%). ¹H NMR (400 MHz, MeOD): δ 8.38 (br s, 1H), 8.21 (d, *J* = 4.9 Hz, 1H), 7.93 (br s, 1H), 7.76 (m, 2H), 7.68 (dd, *J* = 9.1, 2 Hz, 1H), 7.57 (dd, *J* = 9.2, 2.2 Hz, 1H), 7.42 (m, 2H), 5.39 (s, 1H), 5.28 (s, 2H), 1.31 (s, 9H). MS (+ES): *m/e* 401 (MH⁺).

3-(2-(4-Pyridyl)ethyl)indole (2). A mixture of 4-vinylpyridine (0.105 g, 1.0 mmol) and indole (0.117 g, 1.0 mmol) in acetic acid (1 mL) was stirred and refluxed for 16 h. The reaction mixture was cooled to room temperature and the solvent removed under reduced pressure. The residue was subjected to purification by flash chromatography on silica, eluting with ethyl acetate and afforded 0.145 g of **2** as a pale yellow solid, (65%). ¹H NMR (400 MHz, DMSO-*d*₆): δ 10.80 (br s, 1H), 8.45 (d, *J* = 6 Hz, 2H), 7.56 (d, *J* = 8 Hz, 1H), 7.32 (d, *J* = 8 Hz, 1H), 7.29 (d, *J* = 6 Hz, 2H), 7.11 (d, *J* = 2 Hz, 1H), 7.08 (t, *J* = 8 Hz, 1H), 6.97 (t, *J* = 8 Hz, 1H), 3.00 (m, 4H); MS (+ES): *m/e* 223 (MH⁺).

3-[2-(2-Chloro-4-pyrimidinyl)ethyl]indole (20). A mixture of 2-chloro-4-vinylpyrimidine (0.14 g, 1.0 mmol) and indole (0.117 g, 1.0 mmol) in acetic acid (1 mL) was stirred and held at 60–80 °C for 16 h. The reaction mixture was cooled to room temperature and the solvent removed under reduced pressure. The residue was subjected to purification by flash chromatography on silica, eluting with ethyl acetate and afforded 0.167 g of **20** as a pale yellow solid (65%). ¹H NMR (400 MHz, DMSO-*d*₆): δ 10.79 (br s, 1H), 8.61 (d, *J* = 5 Hz, 1H), 7.53 (d, *J* = 8 Hz, 1H), 7.47 (d, *J* = 5 Hz, 1H), 7.32 (d, *J* = 8 Hz, 1H), 7.11 (d, *J* = 2 Hz, 1H), 7.06 (t, *J* = 8 Hz, 1H), 6.97 (t, *J* = 8 Hz, 1H), 3.12 (m, 4H); MS (+ES): *m/e* 258 (MH⁺).

3-(2-(4-Pyrimidinyl)ethyl)indole (19). A mixture of **20** (0.09 g, 0.35 mmol), 10% palladium on carbon (20 mg) and triethylamine (0.07 g, 0.7 mmol) in ethanol (2 mL) was stirred at room temperature under an atmosphere of hydrogen for 16 h. The mixture was filtered, evaporated and the resulting

residue subjected to column chromatography on silica. Elution with diethyl ether afforded 0.064 g of **19** as a pale yellow solid (82%). ¹H NMR (400 MHz, DMSO-*d*₆): δ 10.77 (br s, 1H), 9.10 (d, *J* = 1 Hz, 1H), 8.63 (d, *J* = 5 Hz, 1H), 7.52 (d, *J* = 8 Hz, 1H), 7.42 (dd, *J* = 5, 1 Hz, 1H), 7.32 (d, *J* = 8 Hz, 1H), 7.09 (s, 1H), 7.06 (t, *J* = 8 Hz, 1H), 6.97 (t, *J* = 8 Hz, 1H), 3.11 (s, 4H); MS (+ES): *m/e* 224 (MH⁺).

1-(2-(4-Pyridyl)ethyl)indole (18). A mixture of 4-vinylpyridine (1.05 g, 10.0 mmol), indole (0.585 g, 5.0 mmol), sodium (0.03 g) and anhydrous copper sulfate (0.03 g) in absolute ethanol (3 mL) was stirred at 130 °C in a sealed tube for 16 h. Upon cooling to room temperature, the solvent was removed under reduced pressure and the residue subjected to purification by flash chromatography on silica. Elution with 5% methanol in ethyl acetate afforded 0.6 g of **18** as a pale yellow oil (54%). ¹H NMR (400 MHz, DMSO-*d*₆): δ 8.41 (d, *J* = 6 Hz, 2H), 7.51 (t, *J* = 7.5 Hz, 2H), 7.27 (d, *J* = 3 Hz, 1H), 7.20 (d, *J* = 6 Hz, 2H), 7.11 (tm, *J* = 7.5 Hz, 1H), 6.99 (tm, *J* = 7.5 Hz, 1H), 6.37 (d, *J* = 3 Hz, 1H), 4.46 (t, *J* = 7.5 Hz, 2H), 3.09 (t, *J* = 7.5 Hz, 2H); MS (+ES): *m/e* 223 (MH⁺).

2-[4-(2-(3-Indolyl)ethyl)-2-pyrimidinylamino]-2-methyl-1-propanol (21). A mixture of **20** (0.055 g, 0.2 mmol) and 2-amino-2-methyl-1-propanol (0.5 mL) was stirred and irradiated with microwaves at 200 °C for 5 min. Upon cooling to room-temperature, water was added, the organics were extracted into ethyl acetate, dried (Na₂SO₄), filtered and evaporated and the resulting residue was subjected to column chromatography on silica. Elution with ethyl acetate afforded 0.03 g of **21** as a pale yellow solid (50%). ¹H NMR (400 MHz, DMSO-*d*₆): δ 10.76 (br s, 1H), 8.11 (d, *J* = 5 Hz, 1H), 7.51 (d, *J* = 8 Hz, 1H), 7.32 (d, *J* = 8 Hz, 1H), 7.10 (s, 1H), 7.06 (t, *J* = 8 Hz, 1H), 6.96 (t, *J* = 8 Hz, 1H), 6.50 (d, *J* = 5 Hz, 1H), 6.31 (br s, 1H), 5.11 (t, *J* = 5.5 Hz, 1H), 3.49 (d, *J* = 5.5 Hz, 2H), 3.05 (t, *J* = 7.5 Hz, 2H), 2.86 (t, *J* = 7.5 Hz, 2H), 1.32 (s, 6H); MS (+ES): *m/e* 311 (MH⁺).

N-(5-Indolyl)-3-fluoro-5-(4-morpholino)benzamide (22). A mixture of 5-aminoindole (0.132 g, 1.0 mmol), 3-fluoro-5-(4-morpholino)benzoic acid (0.225 g, 1.0 mmol), 1-hydroxybenzotriazole (0.15 g, 1.1 mmol) and 1-(3-dimethylaminopropyl)-3-ethylcarbodiimide hydrochloride (0.21 g, 1.1 mmol) in DMF (5 mL) was stirred at room temperature for 16 h. The solvent was removed under reduced pressure and the residue partitioned between water and ethyl acetate. The organic layer was separated, dried (Na₂SO₄), filtered, and evaporated and the residue purified by column chromatography on silica. Elution with 50% diethyl ether in petroleum ether afforded 0.25 g of **22** as a colorless foam (74%). ¹H NMR (400 MHz, CDCl₃): δ 8.25 (br s, 1H), 7.94 (s, 1H), 7.81 (br s, 1H), 7.38 (d, *J* = 8.5, 1H), 7.34 (d, *J* = 8.5, 1H), 7.24 (m, 2H), 6.98 (d, *J* = 8.5, 1H), 6.72 (dt, *J* = 11.5, 2, 1H), 6.56 (t, *J* = 2, 1H), 3.86 (m, 4H, m), 3.23 (m, 4H). MS (+ES): *m/e* 340 (MH⁺).

N-[1-(2-(4-Pyridyl)ethyl)-5-indolyl]-3-fluoro-5-(4-morpholino)benzamide (23). A mixture of 4-vinylpyridine (0.078 g, 0.74 mmol) and **22** (0.25 g, 0.74 mmol) in acetic acid (1 mL) was stirred and held at reflux for 16 h. Upon cooling to room temperature, the solvent was removed under reduced pressure and the residue subjected to purification by flash chromatography on silica gel. Elution with ethyl acetate afforded 0.08 g of **23** as a colorless solid (24%). ¹H NMR (400 MHz, DMSO-*d*₆): δ 10.77 (br s, 1H), 10.07 (br s, 1H), 8.44 (d, *J* = 6, 2H), 7.96 (d, *J* = 2, 1H), 7.39 (dd, *J* = 9, 2, 1H), 7.36 (t, *J* = 2, 1H), 7.30 (d, *J* = 8.5, 1H), 7.27 (d, *J* = 6, 2H), 7.17 (dm, *J* = 9, 1H), 7.09 (d, *J* = 2, 1H), 6.98 (dt, *J* = 12, 2, 1H), 3.76 (m, 4H), 3.24 (m, 4H), 2.99 (s, 4H). MS (+ES): *m/e* 445 (MH⁺).

6-Amino-1-(2-(4-pyridyl)ethyl)indole (25). A mixture of 4-vinylpyridine (0.525 g, 5.0 mmol), 6-aminoindole (0.33 g, 2.5 mmol), sodium (0.03 g) and anhydrous copper sulfate (0.03 g) in absolute ethanol (2 mL) was stirred at 130 °C in a sealed tube for 16 h. Upon cooling to room temperature, the solvent was removed under reduced pressure and the residue subjected to purification by flash chromatography on silica. Elution with 5% methanol in ethyl acetate afforded 0.08 g of **25** as a dark brown oil (14%). ¹H NMR (400 MHz, DMSO-*d*₆): δ 8.44 (d, *J* = 6, 2H), 7.21 (d, *J* = 6, 2H), 7.17 (d, *J* = 8, 1H),

6.88 (d, $J = 3$, 1H), 6.60 (d, $J = 2$, 1H), 6.41 (dd, $J = 8$, 2, 1H), 6.13 (d, $J = 3$, 1H), 4.77 (br s, 2H), 4.24 (t, $J = 7.5$, 2H), 3.04 (t, $J = 7.5$, 2H). MS (+ES): m/e 238 (MH⁺).

N-[1-(2-(4-Pyridyl)ethyl)-6-indolyl]-3-fluoro-5-(4-morpholino)benzamide (24). A mixture of **25** (0.048 g, 0.2 mmol), 5-(3-fluoro-5-(4-morpholino)benzoic acid (0.045 g, 0.2 mmol), 1-hydroxybenzotriazole (0.03 g, 0.22 mmol) and 1-(3-dimethylaminopropyl)-3-ethylcarbodiimide hydrochloride (0.043 g, 0.22 mmol) in DMF (2 mL) was stirred at room temperature for 16 h. The solvent was removed under reduced pressure and the residue partitioned between water and ethyl acetate. The organic layer was dried (Na₂SO₄), filtered, and evaporated and the residue purified by column chromatography on silica. Elution with ethyl acetate afforded 0.024 g of **24** as a pale yellow solid (27%). ¹H NMR (400 MHz, DMSO-*d*₆): δ 10.24 (br s, 1H), 8.50 (d, $J = 6$, 2H), 8.11 (br s, 1H), 7.55 (d, $J = 8.5$, 1H), 7.42 (br s, 1H), 7.37 (dd, $J = 8.5$, 1.5, 1H), 7.26 (m, 4H), 7.06 (dt, $J = 12.5$, 2, 1H), 6.40 (d, $J = 3$, 1H), 4.48 (t, $J = 7$, 2H), 3.83 (t, $J = 5$, 4H), 3.31 (t, $J = 5$, 4H), 3.18 (t, $J = 7$, 2H). MS (+ES): m/e 445 (MH⁺).

p38 α Kinase Activity Assays. p38 α Kinase Enzyme Assay. Activity was determined by an enzymatic assay developed in-house: 17 μ g of p38 α (produced in-house) was activated overnight by 0.06 μ g MKK6 (Upstate Discovery) in 25 mM HEPES pH 7.4, 25 mM β -glycerophosphate, 5 mM EDTA, 15 mM MgCl₂, 100 μ M ATP, 1 mM sodium orthovanadate, 1 mM DTT. The activated enzyme (diluted to 10nM) was incubated with 5 μ g of myelin basic protein in 25 μ L of 25 mM HEPES pH 7.4, 25 mM β -glycerophosphate, 5 mM EDTA, 15 mM MgCl₂, 70 μ M ATP, 1 mM sodium orthovanadate, 1 mM DTT, and 0.35 μ Ci of ³³P γ -ATP for 50 min. Compounds and controls were included in a DMSO concentration of 10%. The reaction was stopped by the addition of 30 μ L of 2% orthophosphoric acid and transferred to Millipore MAPH filter plates, prewetted with 50 μ L of 0.5% orthophosphoric acid. The plates were filtered and washed twice with 200 μ L of 0.5% orthophosphoric acid. Incorporated radioactivity was measured by scintillation counting and IC₅₀s were calculated from replicate curves using GraphPad Prism software.

THP-1 Cell Assay for Inhibition of LPS-Induced TNF- α Production. Cell Culture and Compound Preparation. THP-1 cells (human monocytic leukaemia cells ECACC #88081201) were maintained in culture medium [RPMI 1640 (Invitrogen) and 2 mM L-glutamine supplemented with 10% fetal bovine serum (Invitrogen)] at approximately 37 °C in humidified 5% CO₂ in stationary culture. The day of the assay, THP-1 cells were then suspended in culture medium containing 50 ng/mL PMA (Sigma), seeded into a 96-well tissue culture plate (IWAKI) at 1 \times 10⁵ cells/well (100 μ L/well) and incubated as described above for approximately 48 h. The medium was then aspirated, the wells were washed twice in phosphate-buffered saline, and 1 μ g/mL LPS (Sigma L4391, from *Escherichia coli* serotype 0111:B4) in culture medium was added (200 μ L/well). Test compounds were reconstituted in DMSO (Sigma) and then diluted with the culture medium such that the final DMSO concentration was 0.1%.

THP-1 Cell Assay. Confluent THP-1 cells (1 \times 10⁵ cells/100 μ L) were aspirated, the wells washed twice in Phosphate Buffered Saline and 1 μ g/mL LPS (Sigma L4391, from *Escherichia coli* serotype 0111:B4) in culture medium added (200 μ L/well). The cells were then treated with 20 μ L aliquots of test solution or medium only with DMSO (solvent control) and incubated for 6 h as described above. Culture supernatants were collected, transferred to clean culture plates and stored at -80 °C until analyzed. The amount of human TNF- α present was determined by a commercially available enzyme-linked immunosorbent assay (ELISA) kit (R&D Systems #DY210) performed according to the manufacturer's instructions.

Data Analysis. The data from two or greater individual assays were combined and analyzed by nonlinear regression to generate a dose-response curve. The calculated IC₅₀ was defined as the concentration of the test compound that caused

a 50% decrease in the maximal inhibition of p38 α activity as measured by TNF- α production.

References

- Han, J.; Lee, J. D.; Bibbs, L.; Ulevitch, R. J. A MAP kinase targeted by endotoxin and hyperosmolarity in mammalian cells. *Science* **1994**, *265*, 808–811.
- Raingaud, J.; Gupta, S.; Rogers, J. S.; Dickens, M.; Han, J.; Ulevitch, R. J.; David, R. J. Characterization of the structure and function of a novel MAP kinase kinase (MKK6). *J. Biol. Chem.* **1996**, *271*, 2886–2891.
- Raingaud, J.; Whitmarsh, A. J.; Barrett, T.; Derijard, B.; Davis, R. J. MKK3- and MKK6-regulated gene expression is mediated by the p38 mitogen-activated protein kinase signal transduction pathway. *Mol. Cell Biol.* **1996**, *16*, 1247.
- Foster, M. L.; Halley, F.; Souness, J. E. Potential of p38 inhibitors in the treatment of rheumatoid arthritis. *Drug News Perspect.* **2000**, *13*, 488–497.
- Rutgeerts, P.; D'Haens, G.; Targan, S.; Vasiliauskas, E.; Hanauer, S. B.; Present, D. H.; Mayer, L.; Van Hogezaand, R. A.; Braakman, T.; DeWoody, K. L.; Schaible, T. F.; Van Deventer, S. J. H. Efficacy and safety of retreatment with anti-tumour necrosis factor antibody (Infliximab) to maintain remission in Crohn's disease. *Gastroenterology* **1999**, *117*, 761–769.
- Badger, A. M.; Bradbeer, J. N.; Votta, B.; Lee, J. C.; Adams, J. L.; Griswold, D. E. Pharmacological profile of SB 203580, a selective inhibitor of cytokine suppressive binding protein/p38 kinase, in animal models of arthritis, bone resorption, endotoxin shock and immune function. *J. Pharm. Exp. Ther.* **1996**, *279*, 1453–1461.
- Feldmann, M.; Brennan, F. M.; Maini, R. N. Role of Cytokines in rheumatoid arthritis. *Annu. Rev. Immunol.* **1996**, *14*, 397–440.
- Lee, J. C.; Laydon, J. T.; McDonnell, P. C.; Gallagher, T. F.; Kumar, S.; Greed, D. A protein kinase involved in the regulation of inflammatory cytokine biosynthesis. *Nature* **1994**, *372*, 739–746.
- Gallagher, T. F.; Fier-Thompson, S. M.; Gargipati, R. S.; Sorenson, M. E.; Smietana, J. M.; Lee, D. 2,4,5-Triarylimidazole inhibitors of IL-1 biosynthesis. *Bioorg. Med. Chem. Lett.* **1995**, *5*, 1171–1176.
- Jarvis, B.; Faulds, D. Etanercept: a review of its use in rheumatoid arthritis. *Drugs* **1999**, *57*, 945–966.
- Garrison, L.; McDonnell, N. D. Etanercept: therapeutic use in patients with rheumatoid arthritis. *Ann. Rheum. Dis.* **1999**, *58* (Suppl. 1), 65–169.
- Carteron, N. L. Cytokines in rheumatoid arthritis: trials and tribulations. *Mol. Med. Today* **2000**, *6*, 315–323.
- Hamilton, K.; St. Clair, E. W. Tumour necrosis factor- α blockade: a new era for effective management of rheumatoid arthritis. *Exp. Opin. Ther. Pat.* **2000**, *1*, 1041–1052.
- Kumar, S.; Boehm, J.; Lee, J. C. p38 MAP kinases: key signaling molecules as therapeutic targets for inflammatory diseases. *Nature Rev. Drug Disc.* **2003**, *2*, 717–726.
- Chakravarty, S.; Dugar, S. Inhibitors of p38 alpha MAP kinase. *Annu. Reports Med. Chem.* **2002**, *37*, 177–186.
- Cirillo, P. F.; Pargellis, C.; Regan, J. The nondiaryl heterocycle classes of p38 MAP kinase inhibitors. *Curr. Topics Med. Chem.* **2002**, *2*, 1021–1035.
- Jackson, P. F.; Bullington, J. L. Pyridinylimidazole based p38 MAP kinase inhibitors. *Curr. Topics Med. Chem.* **2002**, *2*, 1011–1020.
- Hartshorn, M. J.; Murray, C. W.; Cleasby, A.; Frederickson, M.; Tickle, I. J.; Jhoti, H. Fragment-based Lead Discovery Using X-ray Crystallography. *J. Med. Chem.* **2005**, *48*, 403–413.
- Oprea, T. I. Current trends in lead discovery: are we looking for the appropriate properties? *J. Comput.-Aided Mol. Des.* **2002**, *6*, 325–334.
- Blundell, T. L.; Jhoti, H.; Abell, C. High-throughput crystallography for lead discovery in drug design. *Nat. Rev. Drug Discovery* **2002**, *1*, 45–54.
- Carr, R.; Jhoti, H. Structure-based screening of low-affinity compounds. *Drug Discovery Today* **2002**, *7*, 522–527.
- Wang, Z.; Canagarajah, B. J.; Boehm, J. C.; Kassisa, S.; Cobb, M. H.; Young, P. R.; Abdel-Meguid, S.; Adams, J. L.; Goldsmith, E. J. Structural Basis of inhibitor selectivity in MAP kinases. *Structure* **1998**, *6*, 1117–1128.
- Bristol, J. A.; Gross, I.; Lovey, R. G. An improved synthesis of 2-Amino-3-alkoxyppyridines by a phase-transfer catalysed ether synthesis. *Synthesis* **1981**, 971–973.
- Thompson, A. M.; Showalter, H. D.; Denny, William A. Synthesis of 7-substituted 3-aryl-1,6-naphthyridin-2-amines and 7-substituted 3-aryl-1,6-naphthyridin-2(1H)-ones via diazotization of 3-aryl-1,6-naphthyridine-2,7-diamines. *J. Chem. Soc., Perkin Trans. 1* **2000**, *12*, 1843–1852.
- Gill, A. New lead generation strategies for protein kinase inhibitors – fragment based screening approaches. *Mini-Rev. Med. Chem.* **2004**, *4*, 301–311.

- (26) Pierce, A. C.; Sandretto, K. L.; Bemis, G. W. Kinase inhibitors and the case for CH \cdots O hydrogen bonds in protein–ligand binding. *Proteins* **2002**, *49*, 567–576.
- (27) Lisnock, J.; Tebben, A.; Frantz, B.; O'Neill, E. A.; Croft, G.; O'Keefe, S. J.; Li, B.; Hacker, C.; de Laszlo, S.; Smith, A.; Libby, B.; Liverton, N.; Hermes, J.; LoGrasso, P. Molecular basis for p38 protein kinase inhibitor specificity. *Biochemistry* **1998**, *37*, 16573–16581.
- (28) Dumas, J.; Hatoum-Mokdad, H.; Sibley, R. N.; Smith, R. A.; Scott, W. J.; Khire, U.; Lee, W.; Wood, J.; Wolanin, D.; Cooley, J.; Bankston, D.; Redman, A. M.; Schoenleber, R.; Caringal, Y.; Gunn, D.; Romero, R.; Osterhout, M.; Paulsen, H.; Housley, T. J.; Wilhelm, S. M.; Pirro, J.; Chien, D.; Ranges, G. E.; Shrikhande, A.; Muzsi, A.; Bortolon, E.; Wakefield, J.; Gianpaolo Ostravage, C.; Bhargava, A.; Chau, T. Synthesis and pharmacological characterization of a potent, orally active p38 kinase inhibitor. *Bioorg., Med. Chem. Lett.* **2002**, *12*, 1559–1562.
- (29) Regan, J.; Capolino, A.; Cirillo, P. F.; Gilmore, T.; Graham, A. G.; Hickey, E.; Kroe, R. R.; Madwed, J.; Moriak, M.; Nelson, R.; Pargellis, C. A.; Swinamer, A.; Torcellini, C.; Tsang, M.; Moss, N. Structure–activity relationships of the p38 α MAP kinase inhibitor 1-(5-*tert*-Butyl-2-*p*-tolyl-2*H*-pyrazol-3-yl)-3-[4-(2-morpholin-4-yl-ethoxy)naphthalen-1-yl]urea (BIRB 796). *J. Med. Chem.* **2003**, *46*, 4676–4686. (b) Regan, J.; Breitfelder, S.; Cirillo, P.; Gilmore, T.; Graham, A. G.; Hickey, E.; Klaus, B.; Madwed, J.; Moriak, M.; Moss, N.; Pargellis, C. A.; Pav, S.; Proto, A.; Swinamer, A.; Tong, L.; Torcellini, C. Pyrazole Urea-based inhibitors of p38 MAP kinase: from lead compound to clinical candidate. *J. Med. Chem.* **2002**, *45*, 2994–3008. (c) Pargellis, C.; Tong, L.; Churchill, L.; Cirillo, P. F.; Gilmore, T.; Graham, A. G.; Grob, P. M.; Hickey, E. R.; Moss, N.; Pav, S.; Regan, J. Inhibition of p38 MAP Kinase by Utilizing a Novel Allosteric Binding Site. *Nat. Struct. Biol.* **2002**, *9*, 268–272.
- (30) Gray, A. P.; Archer, W. L. The Pyridylethylation of Indole and Related Reactions. *J. Am. Chem. Soc.* **1957**, *79*, 3554–3559.
- (31) Trejo, A.; Arzeno, H.; Browner, M.; Chanda, S.; Cheng, S.; Comer, D. D.; Dalrymple, S. A.; Dunten, P.; Lafargue, J.; Lovejoy, B.; Friere-Moar, J.; Lim, J.; McIntosh, J.; Miller, J.; Papp, E.; Reuter, D.; Roberts, R.; Sanpablo, F.; Saunders, J.; Song, K.; Villasenor, A.; Warren, S. D.; Welch, M.; Weller, P.; Whiteley, P. E.; Zeng, L.; Goldstein, D. M. Design and Synthesis of 4-Azaindoles as Inhibitors of p38 MAP Kinase. *J. Med. Chem.* **2003**, *46*, 4702–4713.
- (32) Liverton, N. J.; Butcher, J. W.; Claiborne, C. F.; Claremon, D. A.; Libby, B. E.; Nguyen, K. T.; Pitzzenberger, S. M.; Selnick, H. G.; Smith, G. R.; Tebben, A.; Vacca, J. P.; Varga, S. L.; Agarwal, L.; Dancheck, K.; Forsyth, A. J.; Fletcher, D. S.; Frantz, B.; Hanlon, W. A.; Harper, C. F.; Hofsess, S. J.; Kostura, M.; Lin, J.; Luell, S.; O'Neill, E. A.; Orevillo, C. J.; Pang, M.; Parsons, J.; Rolando, A.; Sahly, Y.; Visco, D. M.; O'Keefe, S. J. Design and Synthesis of Potent, Selective and Orally Bioavailable Tetra-substituted Imidazole Inhibitors of p38 Mitogen-Activated Protein Kinase. *J. Med. Chem.* **1999**, *42*, 2180–2190.
- (33) Refined crystallographic coordinates for the structures of p38 α complexed with **1**, **2**, **5**, **9**, **10**, **16**, **22**, **23** and **24** have been deposited with the Protein Data Bank (www.rcsb.org) with entry codes 1w7h, 1w84, 1wbw, 1w83, 1wbn, 1w82, 1wbv, 1wbs, 1wbt, respectively. PDB code for SB203580 is 1a9u.
- (34) Wang Z.; Harkins P. C.; Ulevitch R. J.; Han J.; Cobb M. H.; Goldsmith E. J. The structure of mitogen-activated protein kinase p38 at 2.1 Å resolution. *Proc Natl Acad Sci U.S.A.* **1997**, *6*, 2327–2332.
- (35) Pflugrath, J. W. The finer things in X-ray diffraction data collection. *Acta Crystallogr. D. Biol. Crystallogr.* **1999**, Oct; *55* (Pt 10), 1718–25.
- (36) Leslie, A.; Powell, H. Collaborative Computational Project, Number 4. The CCP4 Suite: Programs for Protein Crystallography. *Acta Crystallogr.* **1994** *D50*, 760–763.
- (37) Brunger, A. T. Free *R* value: A novel statistical quantity for assessing the accuracy of crystal structures. *Nature* **1992**, *355*, 472–475.
- (38) Murshudov, G. N., Vagin, A.A and Dodson, E. J. Refinement of Macromolecular Structures by the Maximum-Likelihood method. *Acta Crystallogr. D.* **2003**, *D53*, 240–255.
- (39) Hartshorn, M. J. A visualization aid for structure based drug design. *J. Comput.-Aided Mol. Des.* **2002**, *16*, 871–881.
- (40) *QUANTA96 X-ray structure analysis, Users Reference*; Molecular Simulations Inc: San Diego, CA, 1996.

JM049575N